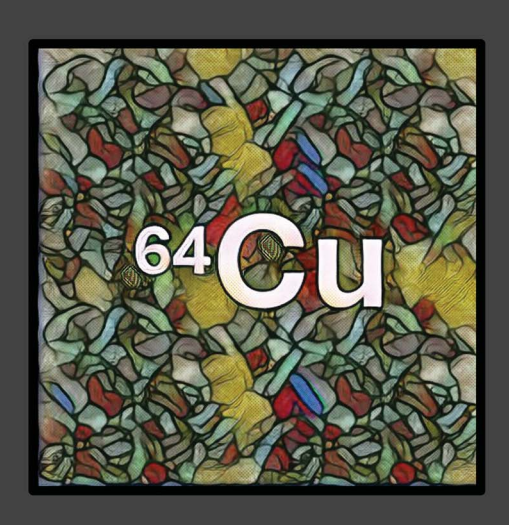
Volume 16 Number 37 7 October 2025 Pages 17005-17508

Chemical Science

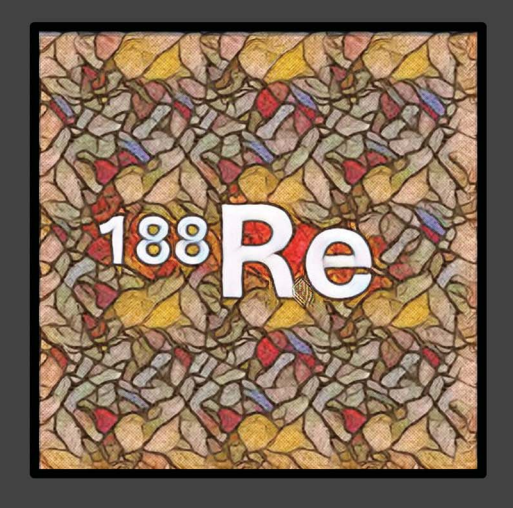
rsc.li/chemical-science











ISSN 2041-6539



EDGE ARTICLE



Chemical Science



EDGE ARTICLE

View Article Online
View Journal | View Issue



Cite this: Chem. Sci., 2025, 16, 17112

dll publication charges for this article have been paid for by the Royal Society of Chemistry

Rachel E. Nuttall, *\bigodot^* a Ingebjørg N. Hungnes, *\alpha Truc T. Pham, *\bigodot^a Oliver W. L. Carter, *\bigodot^a Alex Rigby, *\bigodot^a Natasha Patel, *\alpha Zilin Yu, *\bigodot^a Julie Cleaver, *\bigodot^b Jennifer D. Young, *\bigodot^a Gary J. R. Cook, *\bigodot^a Lefteris Livieratos, *\bigodot^a C Jane Sosabowski, *\bigodot^b Hong Hoi Ting, *\bigodot^a Nicholas Vetter, *\alpha Paul G. Pringle *\bigodot^a and Michelle T. Ma *\bigodot^* a

Maleic anhydride derived diphosphines: adaptable chelators for receptor-targeted ^{99m}Tc, ⁶⁴Cu and

¹⁸⁸Re radiotracers

The diagnostic imaging radionuclide, 99mTc, used in Single Photon Emission Computed Tomography (SPECT), has extraordinary potential for enabling economical molecular receptor imaging in oncology, provided suitable chelators are available to enable kit-based radiolabelling. We report the development of two new bis(phosphino)maleic anhydrides, DPAn and DPMEP, that exhibit increased electron donor capacity and concomitant increased radiochemical yields compared to their first-generation diphosphine analogues. Both DPAn and DPMEP can be reacted with a wide range of biological targeting vectors, including receptor-targeted peptides, carbohydrates, vitamins and small-molecule inhibitors. Exemplar diphosphine-peptide bioconjugates, DPAn-PSMAt and DPMEP-PSMAt (which target the prostate-specific membrane antigen, PSMA), can be formulated into kits to enable near-quantitative, one-pot radiosynthesis of new 99mTc radiotracers, cis/trans-[99mTcO₂(DPAn-PSMAt)₂]+ and cis/trans-[99mTcO₂(DPMEP-PSMAt)₂]⁺, respectively. We demonstrate that the two exemplar 99mTc radiotracers, cis/ trans-[99mTcO₂(DPAn-PSMAt)₂]+ and cis/trans-[99mTcO₂(DPMeP-PSMAt)₂]+, display favourable SPECT imaging properties in murine prostate cancer models, including high tumour uptake, fast clearance from circulation, excretion via a renal pathway and high metabolic stability. The same diphosphine-peptide bioconjugates can also be radiolabelled with the Positron Emission Tomography (PET) isotope, ⁶⁴Cu, and the radiotherapeutic β^- -emitting isotope, ¹⁸⁸Re, in high radiochemical yields. The new DP^{An} and DP^{MEP} chelator platforms thus enable development of novel molecular imaging radiopharmaceuticals for 99mTc SPECT, ⁶⁴Cu PET and ¹⁸⁸Re systemic radiotherapy.

Received 18th March 2025 Accepted 13th August 2025

DOI: 10.1039/d5sc02110c

rsc.li/chemical-science

Introduction

In oncology, receptor-targeted molecular imaging using Single Photon Emission Computed Tomography (SPECT) or γ -scintigraphy has utility in diagnosis, disease staging and clinical decision-making. One class of radiotracer used for this purpose consists of a peptide attached to a chelator, which in turn is complexed to a radioactive metal ion. Two of the most prominent SPECT radiotracers employed for this purpose are 111 In-

DTPA-octreotide and 99m Tc-EDDA/HYNIC-octreotide: both target the somatostatin receptor 2 that is overexpressed in neuroendocrine cancers. Whilst SPECT/ γ -scintigraphy procedures with these radiotracers have been superseded in some healthcare settings by more sensitive Positron Emission Tomography (PET) imaging coupled with the PET radiotracer 68 Ga-DOTA-octreotate, they are still widely used in many clinics where PET is not available.

There are several factors that have led to the prevalence of SPECT/ γ -scintigraphy imaging procedures. First, worldwide, there is simply more SPECT and γ -scintigraphy infrastructure than PET infrastructure, including in lower and middle income countries.³⁻⁶ Second, ^{99m}Tc ($t_{\frac{1}{2}}=6$ h; 90% γ , 140 keV) is widely distributed and available from bench-top ⁹⁹Mo/^{99m}Tc generators in the form of ^{99m}TcO₄ $^-$ in aqueous saline solution.^{5,6} Third, ^{99m}Tc radiotracers, which are routinely used in 30–40 million procedures globally each year, are produced using simple one- or two-step kits in near-quantitative radiochemical yields.⁵⁻⁷

[&]quot;School of Bioengineering and Imaging Sciences, King's College London, 4th Floor Lambeth Wing, St Thomas' Hospital, London, SE1 7EH, UK. E-mail: rachel.nuttall@ kcl.ac.uk; michelle.ma@kcl.ac.uk

^bCentre for Cancer Biomarkers and Biotherapeutics, Barts Cancer Institute, Queen Mary University of London, John Vane Science Centre, Charterhouse Square, London, EC1M 6BQ, UK

Department of Nuclear Medicine, Guy's and St Thomas' Hospitals NHS Foundation Trust, Guy's Hospital, London, SE1 9RT, UK

^dOncobeta GmbH, 85748 Garching, Munich, Germany

eSchool of Chemistry, University of Bristol, Cantock's Close, Bristol, BS8 1TS, UK

Edge Article Chemical Science

Kits for the preparation of ^{99m}Tc radiopharmaceuticals typically contain buffering salts, a reducing agent to reduce ^{99m}Tc^{VII}O₄⁻, a chelator derivative that ultimately complexes the ^{99m}Tc metal ion to form the desired radiopharmaceutical, and other reagents including weak chelators, which serve to stabilise ^{99m}Tc intermediates.^{5,7} The majority of ^{99m}Tc radiopharmaceuticals are for imaging perfusion or anatomical processes.^{5,7} Molecular imaging using ^{99m}Tc-EDDA/HYNIC-octreotide is not as prevalent, in part because of the low incidence of neuroendocrine cancer.

However, recognising the utility and availability of molecular SPECT/γ-scintigraphy infrastructure, in recent years, several new ^{99m}Tc-labelled peptides have been clinically evaluated for receptor-targeted molecular imaging of the prostate-specific membrane antigen (PSMA) overexpressed in prostate cancer. These include ^{99m}Tc-MIP-1404 (also known as ^{99m}Tc-Trofolastat),^{8,9,99m}Tc-PSMA-I&S^{10,11} and ^{99m}Tc-EDDA/HYNIC-iPSMA,^{12,13} which have been shown to be viable alternatives to efficacious PET diagnostic agents that similarly target PSMA.

There is an additional incentive for development of 99mTc radiotracers: in some cases, chemically analogous Re complexes are accessible, providing access to pairs of "theranostic" 99mTc and ¹⁸⁸Re radiopharmaceuticals for diagnosis and therapy, respectively. The rhenium radionuclide, ¹⁸⁸Re ($t_{\pm} = 17$ h; 100% β^- , $E_{\text{max}} = 2.12$ MeV; 15% γ , 155 keV), which can also be produced from a bench-top generator like 99mTc, emits cytotoxic β^- particles. ¹⁸⁸Re radiopharmaceuticals can be effective therapeutics. For example, the lipophilic ¹⁸⁸Re-labelled radiopharmaceutical ¹⁸⁸Re-lipiodol is not only clinically efficacious for treatment of inoperable liver cancer,14 but is also economically viable in lower and middle income countries where supplies of other β-emitting radiopharmaceuticals are limited due to economical and/or geographical barriers. 15,16 Indeed, a newly developed pair of 99mTc/188Re-labelled PSMA-GCK01 theranostic agents has shown favourable properties in preclinical and initial first-in-human studies,17 demonstrating the feasibility of molecular imaging and therapeutic ^{99m}Tc/¹⁸⁸Re pairs.

We have recently explored diphosphine derivatives as potential platforms for radiolabelling receptor-targeted biomolecules. 18-21 These diphosphines include 2,3-bis(diphenylphosphino)maleic anhydride (DPPh)22,23 and 2,3-bis(di-p-tolylphosphino)maleic anhydride (**DP**^{Tol}) (Fig. 1) which react with the primary amine groups of peptides to furnish diphosphine-peptide (DP-peptide) conjugates.18-20† The DP-peptide derivatives coordinate [TcO₂]⁺ or [ReO₂]⁺ motifs to yield complexes of the type cis/trans-[MO₂(**DP-peptide**)₂]⁺ (M = Tc, Re); radiolabelled ^{99m}Tc and ¹⁸⁸Re isotopologues are also synthetically accessible. We have also demonstrated that the resulting 99mTc and 188Re radiotracers retain affinity for their cognate target receptors in vitro and in vivo, and have favourable biodistribution pathways including rapid clearance from the bloodstream via a renal pathway. 18,20 We note that these derivatives also coordinate the PET imaging isotope, ⁶⁴Cu ($t_{\frac{1}{5}}$ = 12.7 h; 18% β^+ , E_{max} = 653 keV), rapidly at room temperature, furnishing radiotracers of formula [Cu(**DP-peptide**)₂]⁺ that show high stability in serum.^{19,22,23}

However, **DP-peptide** derivatives of **DP^{Ph}** do not provide ^{99m}Tc radiotracers in sufficiently high radiochemical yield to enable preparation using a one-step kit without subsequent purification to remove unreacted ^{99m}Tc precursors.¹⁹ Furthermore, radiochemical yields of ¹⁸⁸Re derivatives are relatively low (<50%).²⁰ **DP-peptide** derivatives of **DP**^{Tol} (which contains *p*-tolyl substituents in place of phenyl groups) have shown increased electron donor capacity and concomitant increased radiochemical yields compared to **DP**^{Ph} derivatives.¹⁹ However, even with the improved reactivity of **DP**^{Tol}, we have not been able to obtain radiochemical yields of [^{99m}TcO₂(**DP-peptide**)₂]⁺ compounds above ~85–90%. This is a barrier to clinical translation.

To address this, we have synthesised two novel diphosphine maleic anhydrides, $\mathbf{DP^{An}}$ and $\mathbf{DP^{MEP}}$ (Fig. 1), which possess either p-anisyl or p-(2-methoxyethoxy)phenyl groups on the phosphines, respectively. Bioconjugates of these diphosphine maleic anhydride platforms enable near-quantitative radiochemical syntheses of $^{99\mathrm{m}}$ Tc radiotracers. In our most comprehensive report yet, we have explored the scope of

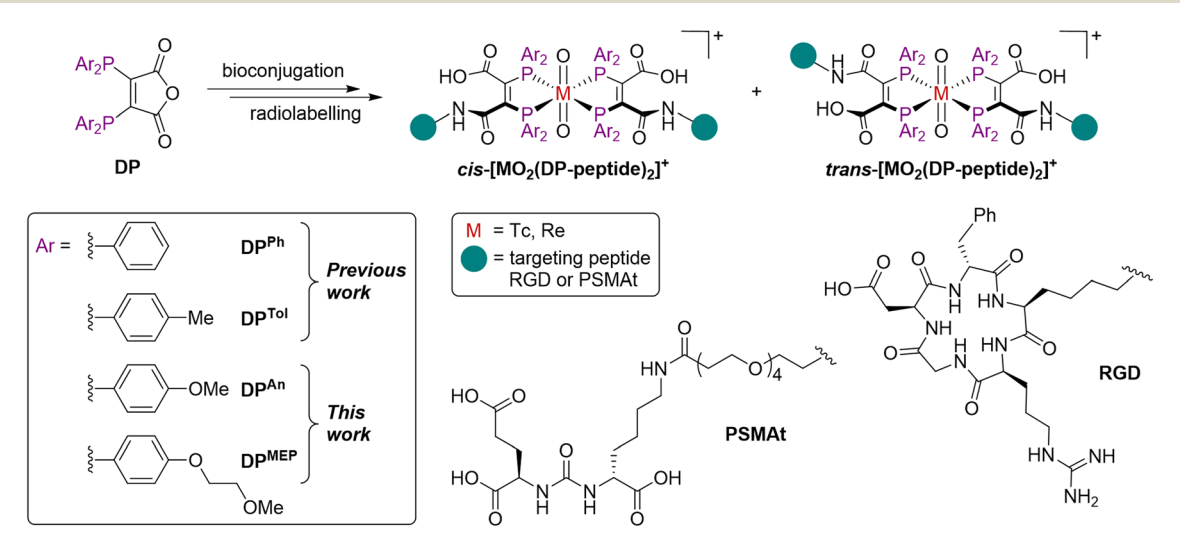


Fig. 1 Structures of cis/trans- $[MO_2(DP-peptide)_2]^+$ complexes, where M = Tc or Re. ^{18–20}

possible bioconjugation reactions with both DP^{An} and DP^{MEP} using a range of biological targeting vectors. We have attached DP^{An} and DP^{MEP} to a PSMA-targeted dipeptide (PSMAt), enabling comparison of DP^{An}-PSMAt and DP^{MEP}-PSMAt with our prior conjugate, DP^{Ph}-PSMAt, including formation of ^{99m}Tc, ¹⁸⁸Re and ⁶⁴Cu complexes. Lastly, our novel ^{99m}Tc radiotracers have been assessed in murine models of prostate cancer using SPECT/CT imaging. We have therefore demonstrated the full utility of our novel and improved DP^{An} and DP^{MEP} platforms for enabling economical and accessible production of pairs of receptor-targeted theranostic radiotracers.

Experimental

Details of experimental procedures are included in the SI. All animal experiments and procedures were ethically reviewed and approved by the Animal Welfare & Ethical Review Boards at either King's College London or Barts Cancer Institute. All animal experiments and procedures were then carried out in accordance with approvals from these committees and review boards, alongside the Animals (Scientific Procedures) Act 1986 UK Home Office regulations governing animal experimentation.

Results

Synthesis of DP^{An} and DP^{MEP} and their PSMAt conjugates

Two novel bis(phosphino)maleic anhydrides were synthesised bearing either p-anisyl ($\mathbf{DP^{An}}$) or p-(2-methoxyethoxy)phenyl

Scheme 1 Synthesis of bis(phosphino)maleic anhydrides, DP^An and DP^MEP

 $(\mathbf{DP^{MEP}})$ substituents. By reaction of the required $\mathrm{Ar_2PH}$ with 2,3-dichloromaleic anhydride in the presence of triethylamine base, $\mathbf{DP^{An}}$ and $\mathbf{DP^{MEP}}$ were synthesised in 89% and 61% yield, respectively (Scheme 1). The syntheses of all precursors, including both diarylphosphines, are described in the SI.

Next, both diphosphines, **DP**^{An} and **DP**^{MEP}, were conjugated to a PSMA-targeting dipeptide, PSMAt-NH₂. Using the pendant primary amine in PSMAt-NH₂ under mild basic conditions, the maleic anhydrides readily ring-opened to form diphosphine bioconjugates, **DP**^{An}-**PSMAt** and **DP**^{MEP}-**PSMAt** in 34% and 37% isolated yield, respectively (Scheme 1). As previously reported for this type of ligand, ^{18,19} **DP**^{An}-**PSMAt** and **DP**^{MEP}-**PSMAt** were stable in the solid state; however, they both slowly oxidised in solution under atmospheric conditions. Under acidic conditions, a reverse reaction occurred to reform **DP**^{An/MEP} and PSMAt-NH₂.

Bioconjugation reactions of $\mathbf{DP}^{\mathbf{An}}$ and $\mathbf{DP}^{\mathbf{MEP}}$ with bioactive small molecules and peptides

To investigate the versatility of this **DP** platform, the reaction of each of **DP**^{An} and **DP**^{MEP} with a range of biologically active amines (Fig. 2) was assessed, including:

- Glucosamine (GlcN), a monosaccharide, as an exemplar carbohydrate;
- Biotin, a vitamin, which binds strongly to streptavidin protein; the biotin/streptavidin pair is used for purification and detection in biotechnology applications;^{24,25}
- Folic acid, a vitamin which targets the folate receptor, overexpressed in ovarian, lung, breast and kidney cancers;^{26,27}
- \bullet RGD, a cyclic pentapeptide, which targets the $\alpha_{v}\beta_{3}$ -integrin receptor overexpressed in inflammation, neovasculature and many cancers;²⁸
- Glutathione (GSH), a thiol-containing antioxidant tripeptide;
- FAPi, a small molecule receptor-targeted inhibitor, which targets the fibroblast activation protein of fibroblastic cells, associated with hard-to-treat cancers (e.g. pancreatic, lung, ovarian cancers).²⁹ Notably, the FAPi motif is a secondary amine (R₂NH), whereas all other amine derivatives above contain primary amines (RNH₂).

The crude reaction mixtures were analysed by LC-MS (Table 1, see SI for full chromatograms). All reactions underwent >95% consumption of the respective DP and/or amine (except for folic acid which showed no reaction). The lack of reactivity of folic acid with either DPAn or DPMEP is presumably due to the low nucleophilicity of the primary amine on the pteridine ring. While both reactions with GSH showed full consumption of DP^{An/MEP}, multiple species were detected by LC-MS. Analysis by ³¹P{¹H} NMR spectroscopy indicated that although the desired amide derivative was formed, additional reactions also occurred, which we attribute to the reactive thiol group of GSH (see SI). When 1-propanethiol was separately reacted with DPAn, multiple ³¹P{¹H} NMR signals with similar chemical shifts were observed. In short, both new **DP**^{An} and **DP**^{MEP} compounds react with thiols to give multiple products: consideration should be taken when a biomolecule with a free thiol group is reacted with these diphosphine compounds.

Fig. 2 Structures of R-NH₂ and RR'-NH amines.

Table 1 Summary of DP-amine conjugations

Entry	DP	$R-NH_2$ or $RR'-NH^a$	DP-X	Expected m/z for $[M + H]^+$	Observed m/z	Conversion ^b
1	$\mathrm{DP}^{\mathrm{An}}$	Biotin-(PEG) ₂ -NH ₂	DP ^{An} -biotin	961.3	961.7	>95%
2		FAPi	DP ^{An} -FAPi	1073.4	1072.9	>95%
3		Folic acid	DP ^{An} -folic acid	1028.3	_	NR^c
4		Glucosamine (GlcN)	DP ^{An} -GlcN	766.2	766.3	>95%
5		Glutathione (GSH)	DP ^{An} -GSH	894.2	894.4	${\sim}83\%^d$
6		RGD	DP ^{An} -RGD	1190.5	1190.8	>95%
7	$\mathbf{DP^{MEP}}$	Biotin-(PEG) ₂ -NH ₂	DP ^{MEP} -biotin	1138.4	1138.0	>95%
8		FAPi	DP ^{MEP} -FAPi	1249.5	1249.8	>95%
9		Folic acid	DP ^{MEP} -folic acid	1204.4	_	NR^c
10		Glucosamine (GlcN)	DP ^{MEP} -GlcN	942.3	942.6	>95%
11		Glutathione (GSH)	DP ^{MEP} -GSH	1070.3	1071.1	${\sim}86\%^d$
12		RGD	DP ^{MEP} -RGD	1366.6	1366.9	>95%

^a RR'–NH only applies to the reaction with FAPi, which contains a secondary amine. ^b Approximate conversion was calculated using the UV signal (280 nm) in HPLC chromatogram(s). See SI for full chromatograms. ^c NR = no reaction. ^d Mixture of products.

Evaluating the donor properties of DP^{An}, DP^{MEP} and derivatives: IR spectra of Mo complexes

The IR stretching frequencies of CO ligands ($\nu_{\rm CO}$) in metal complexes can be used to assess the binding properties of ligands, and complexes of the type cis-[Mo(CO)₄L₂] have previously been utilised for this purpose.³⁰ Strong σ -donors, such as phosphines, increase π -back-bonding from Mo to CO ligands, resulting in lower CO stretching frequencies.

Ligands $\mathbf{DP^{An}}$ and $\mathbf{DP^{MEP}}$, alongside the progenitor $\mathbf{DP^{Ph}}$ (for comparison) were reacted with $\mathit{cis}\text{-}[\mathrm{Mo(CO)_4(nbd)}]$ to give $\mathit{cis}\text{-}[\mathrm{Mo(CO)_4(DP)}]$ complexes (Scheme 2). Additionally, each of these complexes was reacted with (2-methoxyethyl)amine (MOE-NH₂) to yield ring-opened compounds of the type $[\mathrm{Mo(CO)_4(DP-NH-MOE)}]^{-}$, ¹⁹ which all contained an amide bond, to model **DP-peptide** conjugate species (Scheme 2). These complexes were isolated as salts of MOE-NH₃⁺.

Scheme 2 Mo(0) complexation of DP ligands to give cis-[Mo(CO)₄(DP)] and subsequent ring-opening to give cis-[Mo(CO)₄(DP-NH-MOE)]⁻.

The IR $\nu_{\rm CO}$ data for these cis-[Mo(CO)₄L₂] complexes (along-side $^{31}{\rm P}\{^1{\rm H}\}$ NMR and selected $^{13}{\rm C}\{^1{\rm H}\}$ NMR data) are shown in Table 2. There was a decrease in $\nu_{\rm CO}$ in the order [Mo(CO)₄(nbd)] > [Mo(CO)₄(DP^{Ph})] > [Mo(CO)₄(DP^{An})] ~ [Mo(CO)₄(DP^{An}-NH-MOE)]^- > [Mo(CO)₄(DP^{An}-NH-MOE)]^- > [Mo(CO)₄(DP^{MeP}-NH-MOE)]^-. Importantly, complexes of DP^{An}-NH-MOE)]^-.

and $\mathbf{DP^{MEP}}$ and their amide conjugates exhibited lower ν_{CO} values compared with analogous $\mathbf{DP^{Ph}}$ complexes, indicating that the new $\mathbf{DP^{An}}$ and $\mathbf{DP^{MEP}}$ ligands possess increased electron donor capacities compared to $\mathbf{DP^{Ph}}$ derivatives.

The $\nu_{\rm CO}$ stretches were all lower for the amide conjugates, $[{\rm Mo(CO)_4(DP^X-NH-MOE)}]^-$ (X = Ph, An, MEP), compared with the precursor species, $[{\rm Mo(CO)_4(DP^X)}]$ (X = Ph, An, MEP), indicating that **DP-NHR** ligands are significantly better electron donating ligands than the highly electron withdrawing bis(phosphino)maleic anhydride precursor ligands.

^{99m}Tc and ¹⁸⁸Re radiolabelling using generator-produced eluate

We next elected to study the reactions of **DP**^{An}-**PSMAt** and **DP**^{MEP}-**PSMAt** derivatives with generator-produced ^{99m}Tc and ¹⁸⁸Re. For this, the **DP**^{An}-**PSMAt** and **DP**^{MEP}-**PSMAt** conjugates were incorporated into lyophilised kits containing all components required for labelling: reducing agent (SnCl₂), stabilising chelator (sodium tartrate) and buffer (sodium bicarbonate) (Table S1).

For 99m Tc radiosyntheses, the kits were reconstituted using generator produced 99m TcO $_4$ ⁻ (200 MBq) in saline solution (500 μ L) alongside an analogous $\mathbf{DP^{Ph}}$ -PSMAt kit for comparison. The mixtures were then heated at 100 °C for 10 min before radio-iTLC and radio-HPLC analyses. Both $[^{99m}$ TcO $_2(\mathbf{DP^{MEP}}$ -PSMAt) $_2]^+$ were consistently formed in

Table 2 Spectroscopic data for Mo complexes of DPPh, DPAn and DPMEP ligands and their derivatives

Compound	$\nu_{\mathrm{CO}}^{a} (\mathrm{cm}^{-1})$	³¹ P{ ¹ H} NMR (ppm)	¹³ C{ ¹ H} NMR (ppm) of M-CO ligands ^d
DP^Ph	_	$-20.5 (s)^b$	_
$\mathrm{DP}^{\mathrm{An}}$	_	-22.3 (s)^{b}	_
DP^{MEP}	_	$-22.4 (s)^{b}$	_
$[Mo(CO)_4(nbd)]$	2041, 1951, 1888		_
$[Mo(CO)_4(\mathbf{DP^{Ph}})]$	2031, ~1939, 1920	51.7 (s) ^b	215.2 (m, CO _{eq}), 208.9
			$(t, {}^{2}J_{P,C} = 8.5 \text{ Hz}, CO_{ax})^{19}$
$[Mo(CO)_4(\mathbf{DP^{An}})]$	$2028, \sim 1932, 1916$	49.0 (s) ^b	215.9–215.5 (m, CO _{eq}), 209.1
			$(t, {}^{2}J_{P,C} = 8.6 \text{ Hz, CO}_{ax})$
$[Mo(CO)_4(\mathbf{DP^{MEP}})]$	2028 , \sim 1932, 1915	$48.9 (s)^b$	215.8–215.4 (m, CO _{eq}), 209.0
,			$(t, {}^{2}J{P,C} = 8.6 \text{ Hz, CO}_{ax})$
$[MOE-NH_3][Mo(CO)_4(\mathbf{DP^{Ph}-NH-MOE})]$	$2024, \sim 1931, 1902$	72.5 (d, $J = 3.3$ Hz), 70.2	217.9 (m, CO _{eq}), 210.0
		$(d, J = 3.3 \text{ Hz})^c$	$(t, {}^{2}J_{P,C} = 8.6 \text{ Hz}, CO_{ax})^{19}$
[MOE-NH3][Mo(CO)4(DPAn-NH-MOE)]	$2023, \sim 1928, 1899$	69.3 (s), 67.4 (s) ^c	218.0–217.5 (m, CO _{eq}), 209.7
NTD.			$(t, {}^{2}J_{P,C} = 8.5 \text{ Hz, CO}_{ax})$
$[MOE-NH_3][Mo(CO)_4(\mathbf{DP^{MEP}-NH-MOE})]$	2021, 1927, 1897	69.1 (d, $J = 2.7$ Hz), 66.4	218.3–217.8 (m, CO _{eq}), 209.8
		$(\mathrm{d},J=2.7\;\mathrm{Hz})^c$	$(t, {}^{2}J_{P,C} = 8.5 \text{ Hz, CO}_{ax})$

 $[^]a~\mathrm{CH_2Cl_2, 1~mg~mL}^{-1},~``\sim"~\mathrm{denotes~shoulder~peak}.~^b~\mathrm{162~MHz, CDCl_3}.~^c~\mathrm{162~MHz, CD_2Cl_2}.~^d~\mathrm{126~MHz~CD_2Cl_2}.$

Table 3 RCYs of [99mTcO₂(DP-PSMAt)₂]⁺ and [188ReO₂(DP-PSMAt)₂]⁺ complexes

Complex	RCY (%)	Mean difference compared to $[^{99 ext{m}} TcO_2(extbf{DP}^{ extbf{Ph}} ext{-PSMAt})_2]^+$
$[^{99m}_{-}TcO_2(\mathbf{DP^{Ph}-PSMAt})_2]^+$	$76.9 \pm 1.9 \ (n=4)$	Comparator
$[^{99}$ mTcO $_2$ (DP ^{An} - PSMAt) $_2]^+$	$95.1 \pm 0.7 \ (n=6)$	Mean difference = 18.2, 95% confidence interval = 15.3 to 21.1%, $p = 0.0001$
$[^{99}$ mTcO ₂ (DP ^{MEP} - PSMAt) ₂] ⁺	$95.3 \pm 1.3 \ (n=7)$	Mean difference = 18.9, 95% confidence interval = 15.9 to 21.8%, $p = 0.0002$
$[^{188}\text{ReO}_2(\mathbf{DP^{An}\text{-}PSMAt})_2]^+$	$84.7 \pm 7.1\% (n = 4)$	_
$[^{188}\text{ReO}_2(\mathbf{DP^{MEP}\text{-}PSMAt})_2]^+$	$83.1 \pm 6.8\% (n = 4)$	_

Edge Article Chemical Science

≥95% RCY (Table 3), whilst side-by-side radiolabelling reactions of **DP**^{Ph}-**PSMAt** yielded <80% RCY. The major radiochemical impurity in these reactions was ^{99m}Tc colloidal species. Analytical reverse-phase radio-HPLC chromatograms of reactions containing either [^{99m}TcO₂(**DP**^{An}-**PSMAt**)₂]⁺ or [^{99m}TcO₂(**DP**^{An}-**PSMAt**)₂]⁺ showed only one major radioactive species, which we attributed to a mixture of *cis*- and *trans*-[^{99m}TcO₂(**DP**^{An}-**PSMAt**)₂]⁺ or *cis*- and *trans*-[^{99m}TcO₂(**DP**^{MEP}-**PSMAt**)₂]⁺ (Fig. 3). Under these HPLC conditions, *cis* and *trans* isomers were not resolved, however using alternative HPLC conditions (*vide infra*), *cis* and *trans* isomers for [^{99m}TcO₂(**DP**^{An}-**PSMAt**)₂]⁺ could be discerned (see Fig. 5).

For ¹⁸⁸Re radiosyntheses, generator-produced ¹⁸⁸ReO₄ ⁻ was first reduced to a ¹⁸⁸Re^V-citrate precursor, using a mixture of sodium citrate and SnCl₂, as previously described. ^{31,32} Then, aqueous solutions of ¹⁸⁸Re^V-citrate (49–130 MBq, 85 μ L) were added to the contents of two kits containing **DP**^{An}-**PSMAt** or **DP**^{MEP}-**PSMAt** (Table S1), and the mixtures heated to 90 °C for 30 min. The radiochemical yield of [¹⁸⁸ReO₂(**DP**^{An}-**PSMAt**)₂]⁺ measured 84.7% \pm 7.1% (n = 4), and [¹⁸⁸ReO₂(**DP**^{MEP}-**PSMAt**)₂]⁺

measured 83.1% \pm 6.8% (n=4). Analytical reverse-phase radio-HPLC chromatograms (Fig. 4) showed that the reaction products, $[^{188}\text{ReO}_2(\mathbf{DP^{An}\text{-}PSMAt})_2]^+$ and $[^{188}\text{ReO}_2(\mathbf{DP^{MEP}\text{-}PSMAt})_2]^+$, formed one major radiochemical species, with the species observed at 2–3 min attributed to unreacted $^{188}\text{ReO}_4^{-}/^{188}\text{ReV}_2$ -citrate precursor(s). Signals attributed to the desired $^{188}\text{Re-radiolabelled}$ products were broadened at the baseline, and it is possible that there are minor $^{188}\text{Re-radiolabelled}$ side products present in this final kit-based reaction solution.

The $\log D_{\rm OCT/PBS}$ of the new ^{99m}Tc and ¹⁸⁸Re radiotracers was measured (Table 4), with radiotracers isolated from unreacted ^{99m}Tc/¹⁸⁸Re precursor where required, prior to partition coefficient studies. The $\log D_{\rm OCT/PBS}$ values of all four new radiotracers were less than -3.0, indicating that all are highly hydrophilic.

^{99g}Tc radiolabelling

To verify that **DP**^{An}-**PSMAt** and **DP**^{MEP}-**PSMAt** form analogous complexes, the long-lived Tc radionuclide, 99g Tc ($t_{\frac{1}{2}} = 2.1 \times 10^5$ years), was utilised.

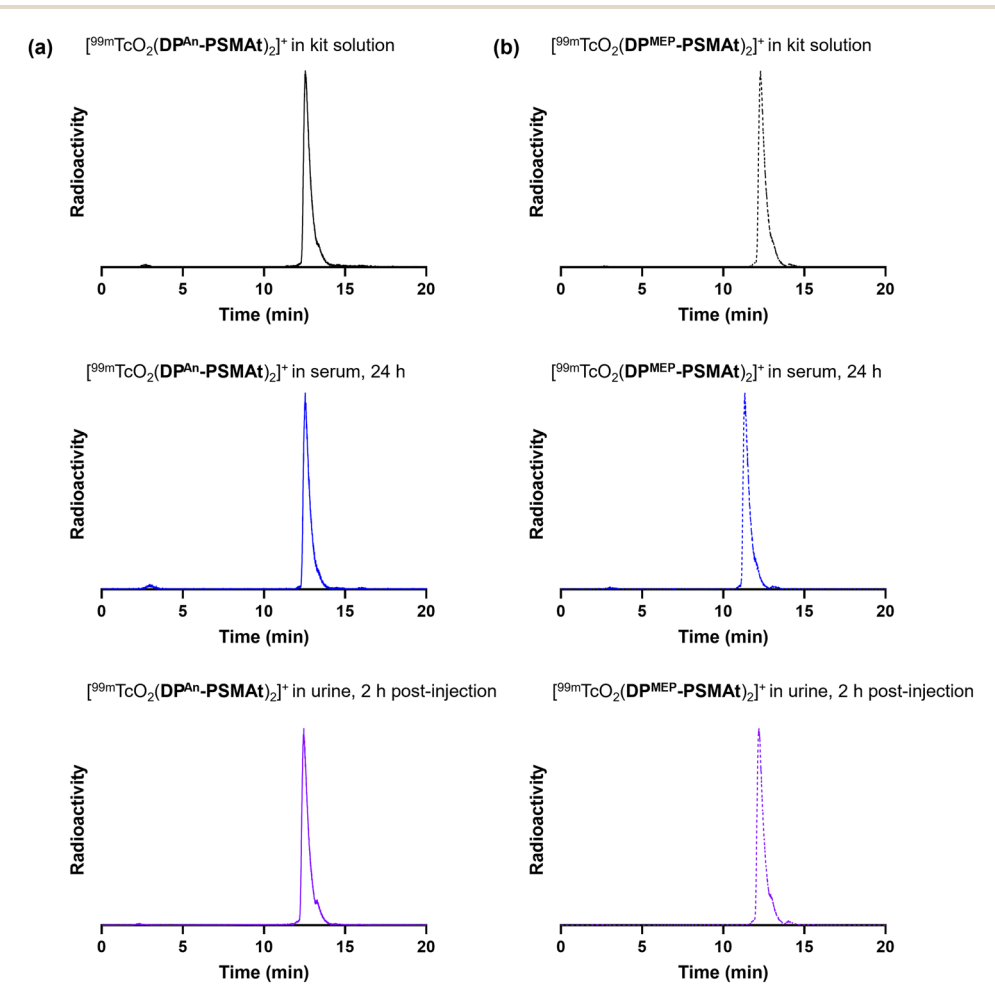


Fig. 3 Radiochromatograms of reactions containing (a) $[^{99m}TcO_2(DP^{An}-PSMAt)_2]^+$ and (b) $[^{99m}TcO_2(DP^{MEP}-PSMAt)_2]^+$, including radiochromatograms of ^{99m}Tc samples after either incubation in human serum at 37 °C, or after administration to a mouse, followed by collection of urine 2 hours post-administration. Radio-HPLC analyses of serum and urine samples indicate that ^{99m}Tc radiotracers possess high stability in the presence of serum proteins and *in vivo*.

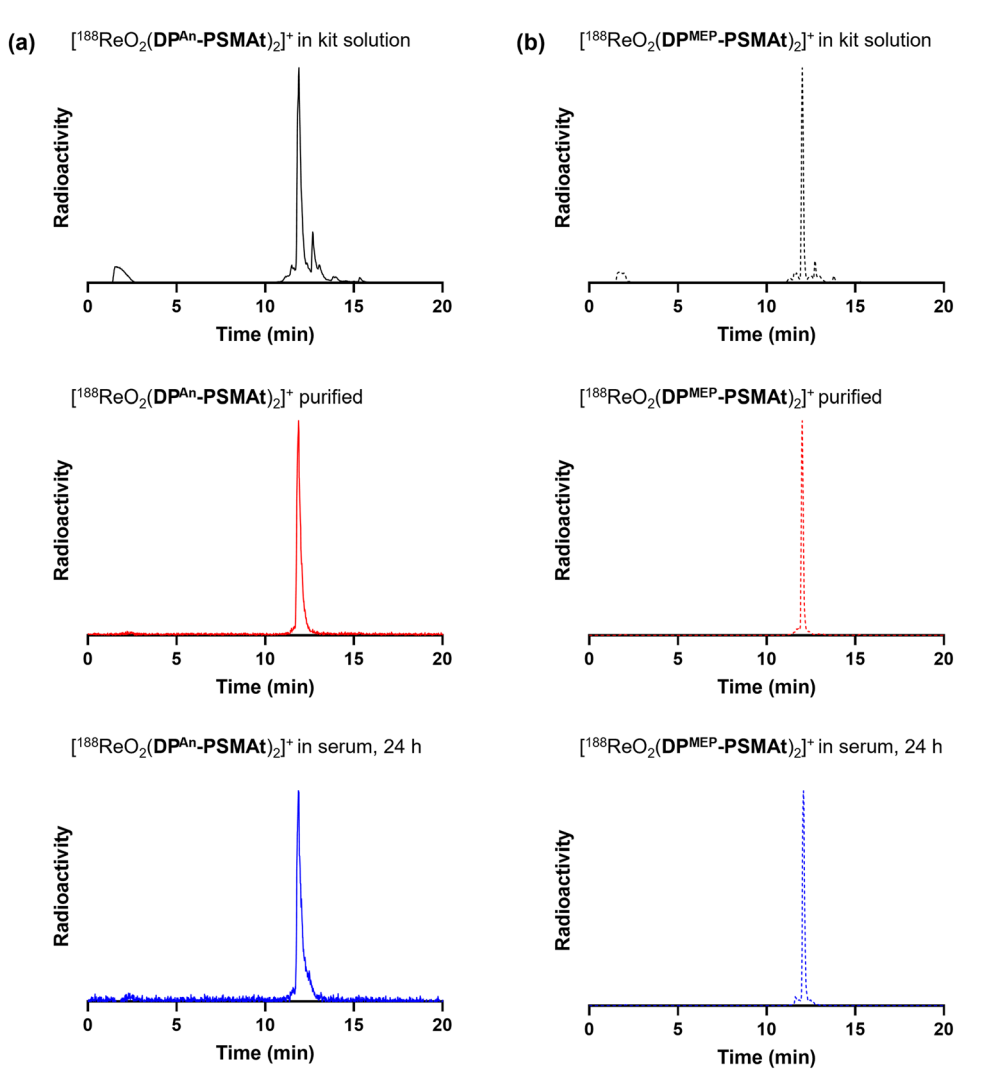


Fig. 4 Radiochromatograms of reactions containing (a) [188ReO₂(DPAn-PSMAt)₂]⁺ and (b) [188ReO₂(DPMEP-PSMAt)₂]⁺, including radiochromatograms of ¹⁸⁸Re-labelled samples after purification and then incubation in human serum at 37 °C. Radio-HPLC analyses of serum samples indicate that 188 Re radiotracers possess high stability in the presence of serum proteins.

Table 4 Log $D_{\rm OCT/PBS}$ values of [MO2(DP-PSMAt)2] $^+$ complexes, where M = $^{99m}{\rm Tc}$ or $^{188}{\rm Re}$

	$\log D_{ m OCT/PBS}$		
	^{99m} Tc	¹⁸⁸ Re	
$\begin{aligned} & \left[\text{MO}_2(\text{DP}^{\text{An}}\text{-PSMAt})_2 \right]^+ \\ & \left[\text{MO}_2(\text{DP}^{\text{MEP}}\text{-PSMAt})_2 \right]^+ \end{aligned}$	$\begin{array}{c} -3.22 \pm 0.04 \\ -3.35 \pm 0.12 \end{array}$	-3.47 ± 0.05 -3.91 ± 0.10	

 $^{99\mathrm{g}}\mathrm{TcO_4}^-$ (0.06 kBq) was reacted with the contents of either a DPAn-PSMAt or DPMEP-PSMAt kit (Table S1), and analysed by LC-MS. Two prominent signals were observed by UV at 330 nm for each kit-based reaction containing either [99gTcO2(DPAn- $PSMAt)_2$ or $[^{99g}TcO_2(DP^{MEP}-PSMAt)_2]^+$ (Fig. 5). The first signal corresponded to the desired product, as evidenced by the appearance of a signal in the associated mass spectrum corresponding to species with a formula of either [99gTcO2(DPAn-**PSMAt**)₂]⁺ ([M + H]²⁺: obs m/z = 1218.8, calc m/z = 1218.9) or $[^{999}\text{TcO}_2(\mathbf{DP^{MEP}\text{-}PSMAt})_2]^+$ ([M + H]²⁺: obs m/z = 1394.9, calc

m/z = 1394.5). The second signal corresponded to that of unreacted DPAn-PSMAt or DPMEP-PSMAt.

Each of $[^{99m}TcO_2(\mathbf{DP^{An}\text{-}PSMAt})_2]^+$, $[^{99m}TcO_2(\mathbf{DP^{MEP}\text{-}PSMAt})_2]^+$, $[^{188}\text{ReO}_2(\mathbf{DP^{An}\text{-}PSMAt})_2]^+$ and $[^{188}\text{ReO}_2(\mathbf{DP^{MEP}\text{-}PSMAt})_2]^+$ was also analysed using the same analytical reverse-phase radio-HPLC (Fig. 5). Analogous ^{99g}Tc, ^{99m}Tc and ¹⁸⁸Re compounds exhibited highly similar HPLC retention times, with tracers based on DP^{An}-PSMAt giving rise to two closely eluting peaks (for $[^{99m}\text{TcO}_2(\mathbf{DP^{An}\text{-}PSMAt})_2]^+$ $t_R = 18.18$ and 18.23 min; for $[^{188}\text{ReO}_2(\mathbf{DP^{An}\text{-}PSMAt})_2]^+$ $t_R = 17.98$ and 18.05 min). We attribute the observation of these two radioactive signals to the formation of cis/trans isomers (Fig. 1). To and Re complexes of DPMEP-PSMAt also likely result in formation of cis/trans isomers, but under these HPLC conditions, these isomers cannot be resolved ($[^{99\text{m}}\text{TcO}_2(\mathbf{DP^{MEP}}\text{-PSMAt})_2]^+$ $t_R = 17.82$ min; for $[^{188}\text{ReO}_2(\mathbf{DP^{MEP}\text{-}PSMAt})_2]^+$ $t_R=17.75$ min). The similar HPLC behaviours of analogous 99mTc and 188Re radiotracers is consistent with analogous pairs of 99mTc/188Re compounds being isostructural.

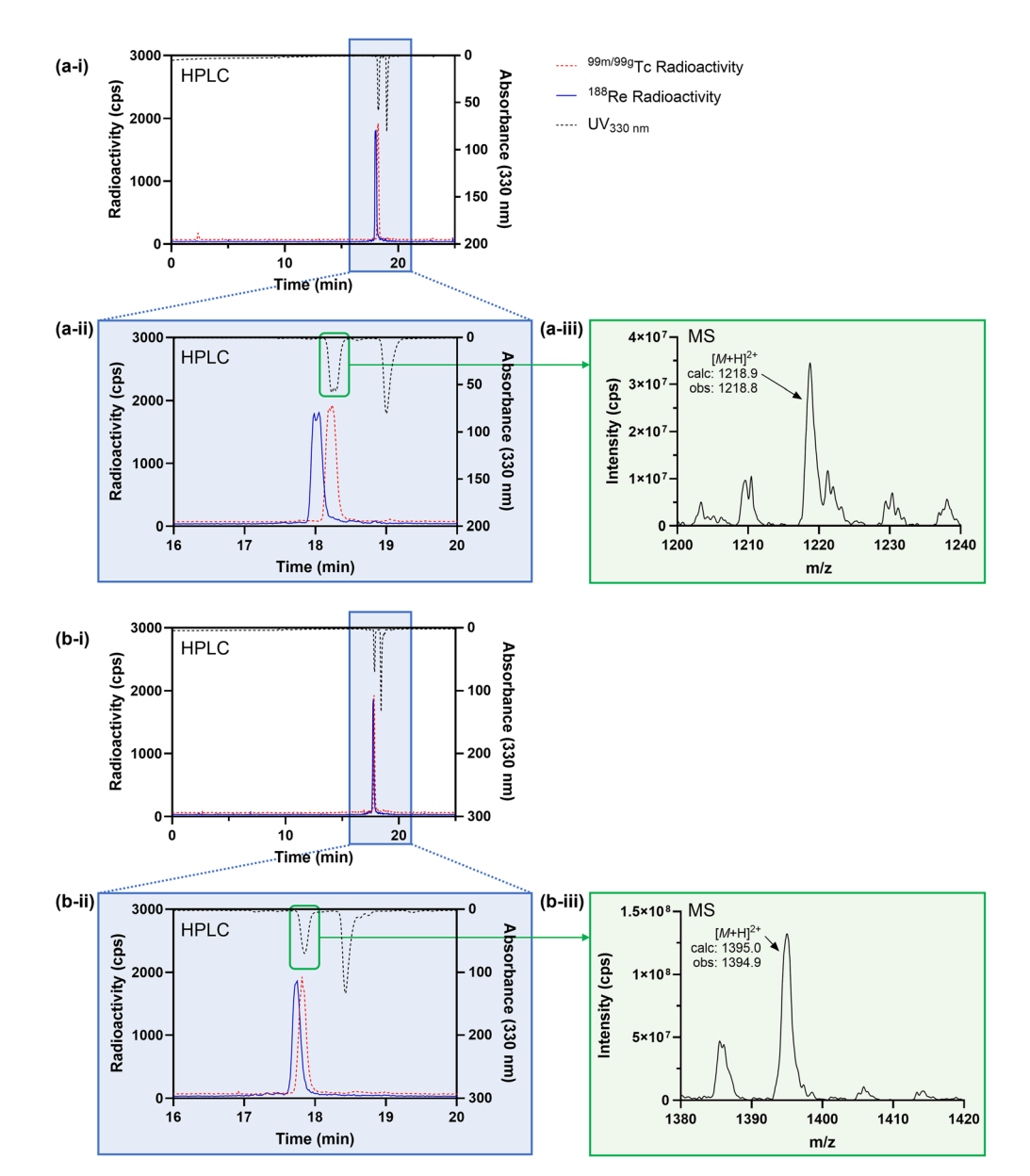


Fig. 5 (a-i) and (a-ii) UV chromatogram and radiochromatograms of reactions containing $[MO_2(DP^{An}-PSMAt)_2]^+$ ($M={}^{99g}Tc$, ${}^{99m}Tc$ or ${}^{188}Re$); (a-iii) mass spectrum showing signal corresponding to $[{}^{99g}TcO_2(DP^{An}-PSMAt)_2]^+$. (b-i and b-ii) UV chromatogram and radiochromatograms of reactions containing $[MO_2(DP^{MEP}-PSMAt)_2]^+$ ($M={}^{99g}TcO_2(DP^{MEP}-PSMAt)_2]^+$ ($M={}^{99g}TcO_2(DP^{MEP}-PSMAt)_2]^+$.

⁶⁴Cu radiolabelling

We and others have previously demonstrated that diphosphines can both (i) reduce ⁶⁴Cu²⁺ to ⁶⁴Cu⁺ in aqueous solution, and (ii) coordinate to the resulting ⁶⁴Cu⁺ radionuclide to yield [⁶⁴Cu(diphosphine)₂]⁺. ^{19,22,23} In these radiochemical reactions, the diphosphine is in large excess compared to the ⁶⁴Cu radiometal.

To demonstrate the utility of these new compounds for radiolabelling with 64 Cu for PET, each of DP^{An} -PSMAt (50.0 µg, 43.3 µmol) and DP^{MEP} -PSMAt (57.7 µg, 43.3 µmol) were reacted with 64 Cu²⁺ (7–8 MBq) in an aqueous solution (0.1 M ammonium acetate, pH 7) at ambient temperature for 10 min. For each reaction, analyses by analytical reverse-phase radio-HPLC (Fig. 6) showed the formation of a single major product,

which we attributed to $[^{64}\text{Cu}(\mathbf{DP^{An}\text{-}PSMAt})_2]^+$ ($t_R = 12.78$ min, 79% RCY), and $[^{64}\text{Cu}(\mathbf{DP^{MEP}\text{-}PSMAt})_2]^+$ ($t_R = 12.67$ min, 87% RCY). The radioactive signals of these products were coincident with the UV signal of the non-radioactive species, $[^{nat}\text{Cu}(\mathbf{DP^{An}\text{-}PSMAt})_2]^+$ ($t_R = 12.71$ min), and $[^{nat}\text{Cu}(\mathbf{DP^{MEP}\text{-}PSMAt})_2]^+$ ($t_R = 12.52$ min), prepared and characterised as described in the SI.¹⁹

The new radiotracers, [⁶⁴Cu(**DP**^{An}-**PSMAt**)₂]⁺ and [⁶⁴Cu(**DP**^{MEP}-**PSMAt**)₂]⁺, were purified using reverse-phase HPLC, reformulated in aqueous PBS (phosphate buffered saline) solution, and incubated with human serum at 37 °C. Radio-HPLC (Fig. 6, and SI) indicated that both [⁶⁴Cu(**DP**^{An}-**PSMAt**)₂]⁺ and [⁶⁴Cu(**DP**^{MEP}-**PSMAt**)₂]⁺ were

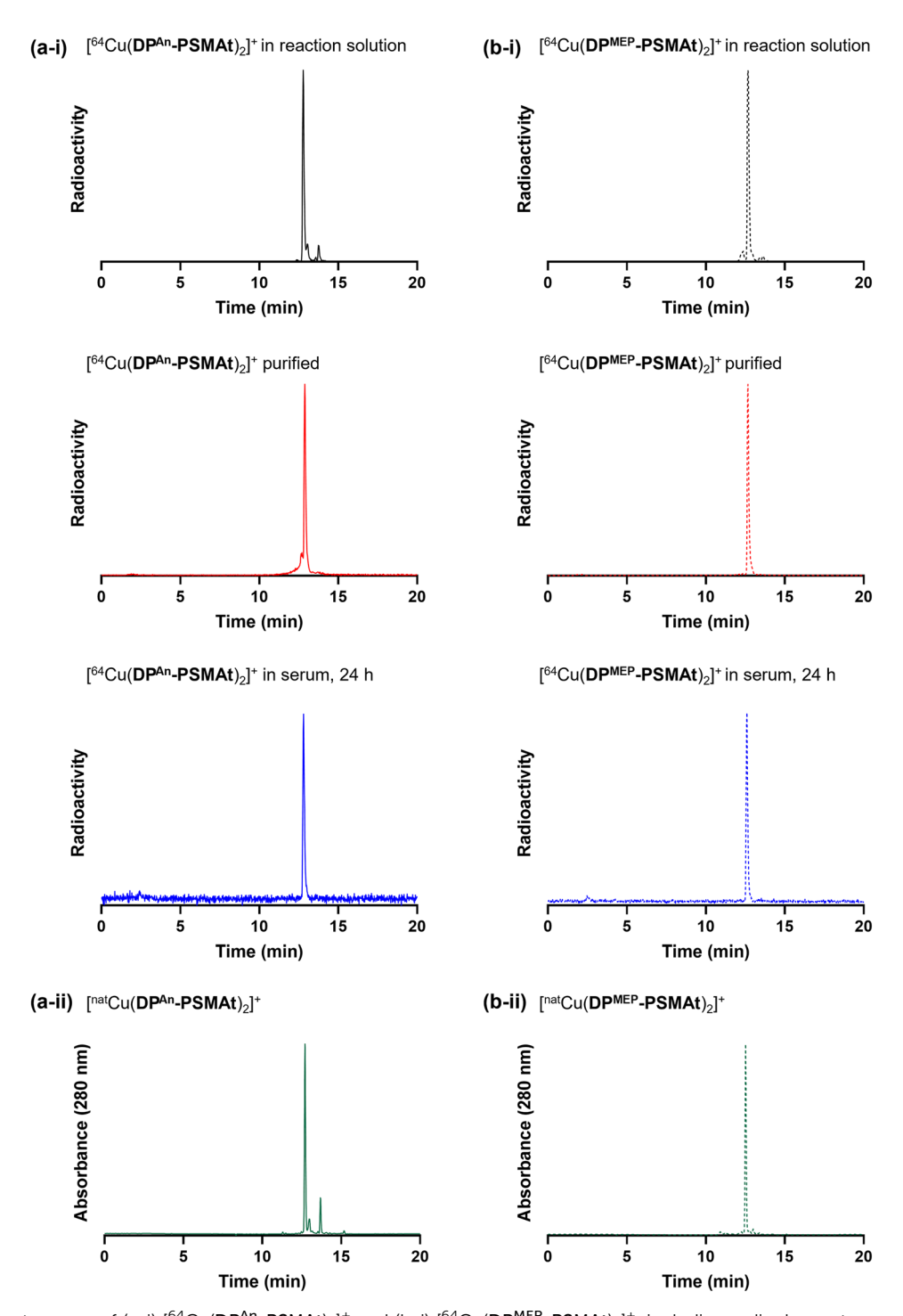


Fig. 6 Radiochromatograms of (a-i) $[^{64}\text{Cu}(DP^{An}-PSMAt)_2]^+$ and (b-i) $[^{64}\text{Cu}(DP^{MEP}-PSMAt)_2]^+$, including radiochromatograms of ^{64}Cu samples after purification and then incubation in human serum at 37 °C. Radio-HPLC analyses of serum samples indicate that ^{64}Cu radiotracers possess high stability in the presence of serum proteins. UV chromatograms of (a-ii) $[^{nat}\text{Cu}(DP^{An}-PSMAt)_2]^+$ and (b-ii) $[^{nat}\text{Cu}(DP^{MEP}-PSMAt)_2]^+$.

present after a 24 h incubation period, with <4.1% dissociated ⁶⁴Cu detected. Both ⁶⁴Cu radiotracers were also stable in aqueous PBS solution (see SI).

In vitro uptake of 99mTc tracers in prostate cancer cells

To compare the relative uptake and specificity of the new radiotracers for PSMA, $[^{99m}TcO_2(\mathbf{DP^{Ph}-PSMAt})_2]^+$,

 $[^{99m}\text{TcO}_2(\mathbf{DP^{An}\text{-}PSMAt})_2]^+$ and $[^{99m}\text{TcO}_2(\mathbf{DP^{MEP}\text{-}PSMAt})_2]^+$ (50 kBq) were purified from unreacted ^{99m}Tc precursors and excess $\mathbf{DP\text{-}PSMAt}$ peptide, and each incubated with PSMA-expressing DU145-PSMA+ prostate cancer cells 33 or LNCaP prostate cancer cells (5 \times 10⁵ cells). After 1 h incubation, uptake of each radiotracer was quantified. Each radiotracer was also (i) co-incubated with the PSMA-inhibitor, PMPA

Edge Article

Fig. 7 In vitro uptake of $[^{99m}TcO_2(DP^{Ph}-PSMAt)_2]^+$, $[^{99m}TcO_2(DP^{Ah}-PSMAt)_2]^+$ and $[^{99m}TcO_2(DP^{MEP}-PSMAt)_2]^+$ radiotracers in PSMA-expressing cell lines (DU145-PSMA+ and LNCaP), in the presence of an excess of PSMA inhibitor (PMPA) in PSMA-expressing cell lines, and in a cell line that does not express PSMA (DU145).

(2-phosphonomethyl pentanedioic acid), in the presence of either DU145-PSMA+ cells or LNCaP cancer cells and (ii) incubated with parental DU145 cells that do not express PSMA. All three radiotracers exhibited uptake in PSMA-expressing prostate cancer cells (Fig. 7). This uptake was specific: DU145-PSMA+ and LNCaP cell uptake of each tracer could be blocked with PMPA, and there was negligible uptake in parental DU145 cells.

The PSMA-specific uptake of $[^{99m}\text{TcO}_2(\mathbf{DP^{Ph}\text{-}PSMAt})_2]^+$ was significantly higher than that of either $[^{99m}\text{TcO}_2(\mathbf{DP^{An}\text{-}PSMAt})_2]^+$ and $[^{99m}\text{TcO}_2(\mathbf{DP^{MEP}\text{-}PSMAt})_2]^+$ in both DU145-PSMA+ cells and LNCaP cancer cells. For example, in DU145-PSMA+ cells, $[^{99m}\text{TcO}_2(\mathbf{DP^{Ph}\text{-}PSMAt})_2]^+$ measured 15.4 \pm 1.9 %AR (% added radioactivity), $[^{99m}\text{TcO}_2(\mathbf{DP^{An}\text{-}PSMAt})_2]^+$ measured 8.9 \pm 2.1 %AR (mean difference = 6.5 %AR, p=0.02) and $[^{99m}\text{TcO}_2(\mathbf{DP^{MEP}\text{-}PSMAt})_2]^+$ measured 2.7 \pm 0.8 %AR (mean difference = 12.7 %AR, p=0.003). The PSMA-specific uptake of $[^{99m}\text{TcO}_2(\mathbf{DP^{MeP}\text{-}PSMAt})_2]^+$ was significantly higher than that of $[^{99m}\text{TcO}_2(\mathbf{DP^{MeP}\text{-}PSMAt})_2]^+$ in both DU145-PSMA+ cells and LNCaP cancer cells. For example, in DU145-PSMA+ cells, mean difference = 6.2 %AR (p=0.03).

In vivo SPECT/CT and biodistribution studies of ^{99m}Tc tracers in mice bearing prostate cancer xenografts

The biodistribution of $[^{99m}\text{TcO}_2(\mathbf{DP^{An}\text{-}PSMAt})_2]^+$ and $[^{99m}\text{TcO}_2(\mathbf{DP^{MEP}\text{-}PSMAt})_2]^+$ was studied using SPECT/CT imaging and $ex\ vivo$ biodistribution methods. In these studies, $[^{99m}\text{TcO}_2(\mathbf{DP^{An}\text{-}PSMAt})_2]^+$ and $[^{99m}\text{TcO}_2(\mathbf{DP^{MEP}\text{-}PSMAt})_2]^+$ were used directly from kit-based formulations, without further purification, mimicking procedures used in clinical radiopharmacies and nuclear medicine departments. Mice were injected with $[^{99m}\text{TcO}_2(\mathbf{DP^{An}\text{-}PSMAt})_2]^+$ or $[^{99m}\text{TcO}_2(\mathbf{DP^{MEP}\text{-}PSMAt})_2]^+$ (4–5 MBq), containing 3 µg (2.6 nmol) of $[^{99m}\text{-}PSMAt]_2$ and culled 2 h post-injection, followed by dissection, organ/tissue weighing and counting.

SPECT/CT studies were undertaken in male SCID/Beige mice bearing DU145-PSMA+ prostate cancer xenografts administered $[^{99}$ mTcO₂(**DP**^{MEP}-**PSMAt**)₂]⁺. $[^{99}$ mTcO₂(**DP**^{An}-**PSMAt**)₂]⁺ and SPECT images were acquired from 15 to 120 min post-injection of radiotracer. In SPECT/CT scans of mice administered either $[^{99}$ mTcO₂(DP^{An}-PSMAt)₂]⁺ or $[^{99}$ mTcO₂(**DP**^{MEP}-**PSMAt**)₂]⁺, tumours (T) could be delineated, with higher tumour to background ratios at later time points (Fig. 8). The kidneys (K) and bladder (B) were also clearly visible across all these timepoints with low background levels, indicating that both the radiotracers are rapidly cleared from the blood pool via a renal pathway.

Quantification of SPECT/CT images (acquired at 15–30 min, 30–60 min, 60–90 min and 90–120 min post-injection, Fig. 8) indicated that tumour uptake of $[^{99m}TcO_2(\mathbf{DP^{An}}-\mathbf{PSMAt})_2]^+$ was higher than that of $[^{99m}TcO_2(\mathbf{DP^{MEP}}-\mathbf{PSMAt})_2]^+$, consistent with *in vitro* uptake studies and *ex vivo* biodistribution data (*vide infra*). Additionally, for the mouse administered $[^{99m}TcO_2(\mathbf{DP^{An}}-\mathbf{PSMAt})_2]^+$, the ^{99m}Tc tumour concentration noticeably increased from 30 min until 2 h post-injection.

SPECT/CT indicated that ^{99m}Tc residualised in salivary glands for animals administered either $[^{99m}TcO_2(\textbf{DP^{An}-PSMAt})_2]^+$ or $[^{99m}TcO_2(\textbf{DP^{MEP}-PSMAt})_2]^+$. Two well-documented mechanisms of radiotracer uptake likely account for salivary gland uptake:

- (i) PSMA is expressed at low levels in the salivary glands, kidneys and small intestine, with PSMA-targeted radiotracers showing uptake in the salivary glands, in both mice and human patients. Indeed, the salivary glands are considered doselimiting organs, and uptake of radiotherapeutic PSMA-targeted radiopharmaceuticals can lead to xerostomia in prostate cancer patients.
- (ii) TcO₄, bearing a single negative charge and with a similar polyatomic radius to that of the iodide anion, acts as a substrate for the sodium iodide symporter in vivo, 37 and therefore accumulates in organs expressing the sodium iodide symporter - in mice, this includes the thyroid, salivary glands and stomach.38 SPECT imaging quantification (consistent with biodistribution data, vide infra) indicated that ^{99m}Tc concentrations were higher in the salivary glands for the mouse administered [99mTcO₂(**DP**^{MEP}-**PSMAt**)₂]⁺ compared to the mouse administered $[^{99m}TcO_2(\mathbf{DP^{An}-PSMAt})_2]^+$. Indeed, 99mTc concentrations in the salivary glands increased over time for the former subject. This suggests that $[^{99m}TcO_2(\mathbf{DP^{MEP}\text{-}PSMAt})_2]^+$ could possess lower *in vivo* stability than [99mTcO₂(DPAn-PSMAt)₂]+, with complex dissociation and oxidation of the [99mTcVO2] motif resulting in formation of ^{99m}TcO₄ - in vivo, and increased ^{99m}Tc accumulation in the salivary glands for animals administered [99mTcO₂(**DP**^{MEP}-**PSMAt**)₂]⁺.

The biodistribution of [99mTcO₂(**DP**^{An}-**PSMAt**)₂]⁺ and [99mTcO₂(**DP**^{MEP}-**PSMAt**)₂]⁺ was further studied in (i) male SCID/Beige mice bearing DU145-PSMA+ prostate cancer xenografts (Fig. 8) and (ii) male nude mice bearing PSMA-expressing LNCaP prostate cancer xenografts (see SI).

For all animals, significant concentrations of 99m Tc radioactivity (2–5 %ID g^{-1}) were measured in PSMA-expressing tumours 2 h post-injection, and although 99m Tc tumour

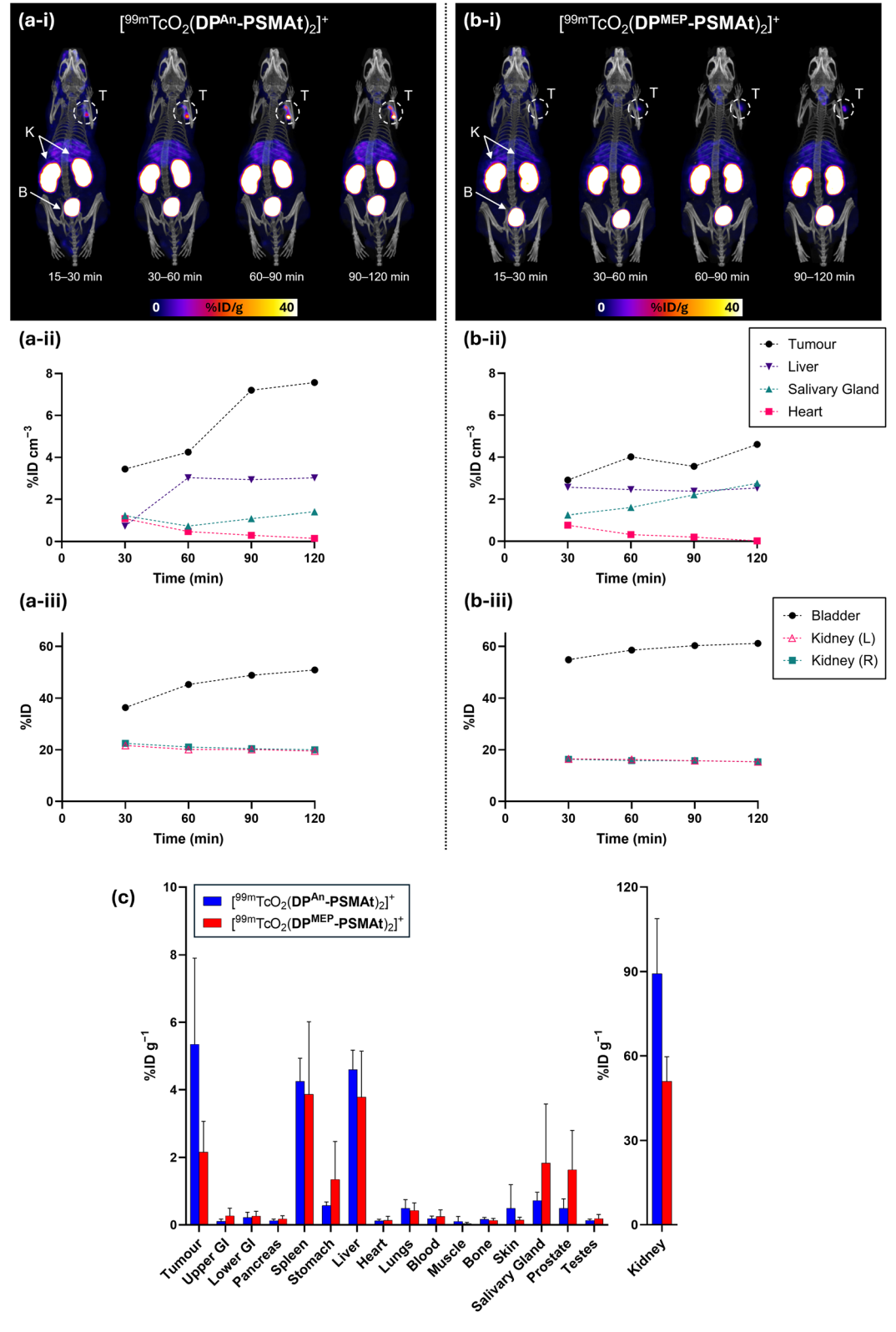


Fig. 8 Whole body SPECT/CT maximum intensity projections and image quantification of SCID/Beige mice bearing DU145-PSMA+ tumours administered either (a) $[^{99m}TcO_2(DP^{An}-PSMAt)_2]^+$ or $[^{99m}TcO_2(DP^{MEP}-PSMAt)_2]^+$. T = tumour, K = kidneys, B = bladder. (c) Biodistribution (2 h post-injection) of $[^{99m}TcO_2(DP^{An}-PSMAt)_2]^+$ or $[^{99m}TcO_2(DP^{MEP}-PSMAt)_2]^+$ in SCID/Beige mice bearing DU145-PSMA+ prostate cancer xenografts (mean \pm SD, n = 3-4).

concentrations were consistently higher for animals administered $[^{99\mathrm{m}}\mathrm{TcO}_2(\mathbf{DP^{An}\text{-}PSMAt})_2]^+$, there were no statistically significant differences between $[^{99\mathrm{m}}\mathrm{TcO}_2(\mathbf{DP^{An}\text{-}PSMAt})_2]^+$ and $[^{99\mathrm{m}}\mathrm{TcO}_2(\mathbf{DP^{MEP}\text{-}PSMAt})_2]^+$ in either mouse model. For both tracers, there were also significant concentrations of $^{99\mathrm{m}}\mathrm{Tc}$ radioactivity in the spleen, which is known to express low levels of PSMA and accumulate PSMA-targeted radiotracers, 9,10 and the liver. Importantly, clearance from the blood pool and subsequent excretion was largely via a renal route, with concentrations of 40–90 %ID g^{-1} measured in kidneys.

We also noted that for both SCID/beige and nude mice studies, higher ^{99m}Tc concentrations were observed in the stomach and salivary glands for animals administered $[^{99m}TcO_2(\mathbf{DP^{MEP}\text{-}PSMAt})_2]^+$ compared to animals administered $[^{99m}TcO_2(\mathbf{DP^{An}\text{-}PSMAt})_2]^+$, although these differences were not statistically significant. This observation is consistent with observations from SPECT/CT imaging studies, and further supports our conjecture that $[^{99m}TcO_2(\mathbf{DP^{MEP}\text{-}PSMAt})_2]^+$ has lower $in\ vivo$ stability than $[^{99m}TcO_2(\mathbf{DP^{An}\text{-}PSMAt})_2]^+$, with $in\ vivo$ formation of $^{99m}TcO_4^-$ from dissociation of $[^{99m}TcO_2(\mathbf{DP^{MEP}\text{-}PSMAt})_2]^+$ resulting in higher levels of $^{99m}Tc\ activity$ in organs expressing the sodium iodide symporter.

Overall, the *in vivo* biodistribution demonstrates that both $[^{99m}TcO_2(\mathbf{DP^{An}\text{-}PSMAt})_2]^+$ and $[^{99m}TcO_2(\mathbf{DP^{MEP}\text{-}PSMAt})_2]^+$ are useful SPECT or γ -scintigraphy imaging agents for PSMA expression in prostate cancer.

Stability of $[MO_2(DP^{An}-PSMAt)_2]^+$ and $[MO_2(DP^{MEP}-PSMAt)_2]^+$ $(M = ^{99m}Te, ^{188}Re)$

Both $[^{99m}\text{TcO}_2(\mathbf{DP^{An}\text{-}PSMAt})_2]^+$ and $[^{99m}\text{TcO}_2(\mathbf{DP^{MEP}\text{-}PSMAt})_2]^+$, prepared using kits, were incubated at 37 °C in human serum for up to 24 h. Analytical reverse-phase radio-HPLC (Fig. 3) demonstrated that >98% of both radiotracers remained intact in serum. $[^{188}\text{ReO}_2(\mathbf{DP^{An}\text{-}PSMAt})_2]^+$ and $[^{188}\text{ReO}_2(\mathbf{DP^{MEP}\text{-}PSMAt})_2]^+$, prepared using kits and then isolated using reverse-phase HPLC in >98% radiochemical purity, were also incubated in human serum under the same conditions. Radio-HPLC (Fig. 4) similarly showed that $^{188}\text{Re-labelled}$ radiotracers were stable in serum over 24 h, with <1.5% of ^{188}Re dissociating over this time. These ^{99m}Tc and ^{188}Re radiotracers were also stable when left to stand in kit-based reaction solutions, or in PBS solution (see SI for full chromatograms).

Urine was also collected in *in vivo* ^{99m}Tc biodistribution experiments (from male SCID/Beige mice bearing DU145-PSMA+ prostate cancer xenografts at 2 h post-injection) and analysed using reverse-phase radio-HPLC (Fig. 3). Radio-chromatograms indicated that both [^{99m}TcO₂(**DP**^{An}-**PSMAt**)₂]⁺ and [^{99m}TcO₂(**DP**^{MEP}-**PSMAt**)₂]⁺ were excreted in urine intact, indicating that both radiotracers have high stability *in vivo*.

Discussion

We have recently reported **DP**^{Ph} and **DP**^{Tol} derivatives of the 2,3-bis(diphenylphosphino)maleic anhydride platform, and shown that the resulting ^{99m}Tc and ¹⁸⁸Re radiotracers have desirable properties as molecular theranostic agents. ^{19,20} Here, we have

optimised this platform technology through development of $\mathbf{DP^{An}}$ and $\mathbf{DP^{MEP}}$, and demonstrated that these compounds can be attached to a variety of amine-containing bioactive molecules, including peptides, carbohydrates, vitamins and small molecule inhibitors. The resulting diphosphine conjugates can be radiolabelled with ^{99m}Tc, ¹⁸⁸Re and ⁶⁴Cu, thus enabling formation of radiotracers for molecular SPECT imaging, radiotherapy and molecular PET imaging, respectively.

Significantly, as hypothesised, the increased σ -donating ability of **DP**^{An} and **DP**^{MEP} derivatives, due to para substituents on aryl rings of the phosphines, leads to further increased RCYs within this family of diphosphine chelators ($\mathbf{DP^{An}} \sim$ $DP^{MEP} > DP^{Tol} > DP^{Ph}$). The kit formulations of DP^{An} and DPMEP conjugates developed here use relatively small amounts of DP^{An}-PSMAt and DP^{MEP}-PSMAt diphosphine bioconjugates (110 nmol, 113-145 µg), minimising competitive target receptor binding of unreacted ligand present in formulations administered to in vivo subjects. The high RCYs (≥95%) of $\lceil ^{99\text{m}}\text{TcO}_2(\mathbf{DP^{An}\text{-}PSMAt})_2 \rceil^+$ and $\lceil ^{99\text{m}}\text{TcO}_2(\mathbf{DP^{MEP}\text{-}PSMAt})_2 \rceil^+$ achieved using our one-step kit formulation negate the need for time-intensive and often complicated purification procedures to remove unreacted 99mTc precursors. In a clinical context, rapid, one-step radiolabelling and formulation protocols using kits are desirable: this simplicity of producing a radiopharmaceutical for immediate patient injection makes widespread clinical adoption feasible. We are yet to optimise ¹⁸⁸Re radiolabelling protocols including kit formulations for new ¹⁸⁸Re radiotracers, however, we note that the radiochemical yields (>83%) are significantly improved compared to RCYs of prior **DP**^{Ph} and **DP**^{Tol} conjugate derivatives.²⁰ In these previous reactions, ¹⁸⁸Re radiotracer yields were often highly variable, and commonly less than 30%.

The $\log D_{\rm OCT/PBS}$ values observed here are all lower than those previously reported for $[^{99\rm m}{\rm TcO_2}({\bf DP^{Ph/Tol}\text{-PSMAt}})_2]^+$ derivatives, consistent with the more hydrophilic methoxy and methyl ethylene glycol substituents of aryl rings, compared to ${\bf DP^{Ph}}$ and ${\bf DP^{Tol}}$ analogues. This also poses potential advantages for receptor-targeted biomolecular vectors that are significantly more hydrophobic than the PSMAt pharmacophore tested here.

We observe decreasing uptake of $[^{99m}TcO_2(DP^X-PSMAt)_2]^+$ (X = Ph, An, MEP) radiotracer analogues in PSMA-positive prostate cancer cells in the order Ph > An > MEP and we note that this corresponds with increasing size and hydrophilicity of the *para* substituents: H < OCH₃ < OCH₂CH₂OCH₃. It is well documented that aromatic groups are important in PSMA affinity, due to the hydrophobic binding pocket of PSMA. 39,40 We postulate that the *para* substituents interfere with binding of the radiotracer to PSMA.

In the biodistribution experiments undertaken for this work, prostate cancer tumour uptake of $[^{99m}TcO_2(\mathbf{DP^{MP}\text{-}PSMAt})_2]^+$ and $[^{99m}TcO_2(\mathbf{DP^{MP}\text{-}PSMAt})_2]^+$ was lower than previously reported for $[^{99m}TcO_2(\mathbf{DP^{Ph}\text{-}PSMAt})_2]^+$ and $[^{99m}TcO_2(\mathbf{DP^{Tol}\text{-}PSMAt})_2]^+$ in the same murine tumour models. 20 This was expected: here, kit-based formulations of $[^{99m}TcO_2(\mathbf{DP^{MP}\text{-}PSMAt})_2]^+$ and $[^{99m}TcO_2(\mathbf{DP^{MP}\text{-}PSMAt})_2]^+$ were not purified from unreacted, excess $\mathbf{DP^{MP}\text{-}PSMAt}$ and $\mathbf{DP^{MPP}\text{-}PSMAt}$ respectively, prior to

Table 5 Comparison of biodistribution of ^{99m}Tc-labeled PSMA-targeted radiotracers

Radiotracer (time post-injection)	$Blood^a$	Liver ^a	Kidney ^a
[99mTcO ₂ (DP^{An}-PSMAt) ₂] ⁺ (athymic nude, 2 h)	0.11 ± 0.04	0.90 ± 0.15	87.6 ± 13.3
$[^{99m}\text{TcO}_2(\mathbf{DP^{MEP}\text{-}PSMAt})_2]^+$ (athymic nude, 2 h)	0.17 ± 0.10	7.38 ± 3.98	46.4 ± 23.2
$[^{99}$ mTcO ₂ (DP ^{Ph} - PSMAt) ₂] ⁺ (athymic nude, 2 h) ²⁰	0.23 ± 0.05	0.35 ± 0.05	203.56 ± 13.67
$[^{99\text{m}}\text{TcO}_2(\mathbf{DP^{Tol}}-\mathbf{PSMAt})_2]^+$ (athymic nude, 2 h) ²⁰	0.28 ± 0.05	0.52 ± 0.05	212.23 ± 29.49
^{59m} Tc-MIP-1404 (athymic nude, 1 h) ⁹	0.13 ± 0.03	0.14 ± 0.03	105 ± 37
^{99m} Tc-PSMA-I&S (SCID, 1 h) ¹⁰	1.73 ± 0.50	1.58 ± 0.24	186 ± 23
^{99m} Tc-EDDA/HYNIC-iPSMA (athymic, 1 h) ¹³	0.18 ± 0.08	2.18 ± 0.19	23.63 ± 3.56
a % ID g $^{-1}$, \pm standard deviation.			

injection. It is likely that **DP**^{An}-**PSMAt** and **DP**^{MEP}-**PSMAt** compete for binding to PSMA receptor *in vivo*.

Liver concentrations of $[^{99m}\text{TcO}_2(\mathbf{DP^{An}\text{-}PSMAt})_2]^+$ and $[^{99m}\text{TcO}_2(\mathbf{DP^{MEP}\text{-}PSMAt})_2]^+$ were observed to be higher than that previously measured for first-generation $[^{99m}\text{TcO}_2(\mathbf{DP^{Ph}\text{-}PSMAt})_2]^+$ and $[^{99m}\text{TcO}_2(\mathbf{DP^{Tol}\text{-}PSMAt})_2]^+$ radiotracers in the same murine models. An increased liver accumulation of a tracer can correlate with increased hydrophobicity of compounds, but we note that $\log D_{\mathrm{OCT/PBS}}$ values indicate that $[^{99m}\text{TcO}_2(\mathbf{DP^{An}\text{-}PSMAt})_2]^+$ and $[^{99m}\text{TcO}_2(\mathbf{DP^{MEP}\text{-}PSMAt})_2]^+$ are both more hydrophilic than their predecessors. We therefore attribute the higher liver accumulation of $[^{99m}\text{TcO}_2(\mathbf{DP^{An}\text{-}PSMAt})_2]^+$ and $[^{99m}\text{TcO}_2(\mathbf{DP^{MEP}\text{-}PSMAt})_2]^+$ to either their increased size, or alternatively, the different formulation of the radiotracer dose, which includes unlabelled bioconjugate precursor, which could affect the biodistribution.

Compared to animals administered [99mTcO2(DPAn- $PSMAt)_2$, animals administered [$^{99m}TcO_2(DP^{MEP}-PSMAt)_2$] presented higher 99mTc concentrations in salivary glands and the stomach. This could indicate that [99mTcO2(DPMEP-**PSMAt**)₂]⁺ exhibits a degree of instability *in vivo*, as both the salivary glands and the stomach express the sodium iodide symporter and are known to take up 99mTcO4-38 It is also possible that some salivary gland uptake is due to known salivary gland PSMA expression.34,35 However, except for the possible formation of small amounts of 99mTcO₄ in vivo, both $[^{99m}TcO_2(\mathbf{DP^{An}\text{-}PSMAt})_2]^+$ $[^{99m}TcO_2(\mathbf{DP^{MEP}\text{-}PSMAt})_2]^+$ and demonstrated high metabolic stability, as evidenced by their excretion intact in urine, and their high stability in serum (ex vivo) over 24 h.

Our new diphosphine chelator technology has advantages over other ^{99m}Tc and ¹⁸⁸Re radiolabelling platforms. For instance, the radiosynthesis and purification of ^{99m}Tc-MIP-1404, which is based on the [^{99m}Tc(CO)₃]⁺ synthon, is time-consuming. It requires (i) formation of an intermediate *fac*-[^{99m}Tc(CO)₃(H₂O)₃]⁺ precursor prior to (ii) chelation with the tridentate MIP-1404 chelator-peptide, and finally (iii) purification and formulation before administration. Other molecular ^{99m}Tc-radiopharmaceuticals, including ^{99m}Tc-EDDA/HYNIC-octreotide and ^{99m}Tc-EDDA/HYNIC-iPSMA, ^{8,9} utilise the 6-hydrazinopyridine-3-carboxylic acid (HYNIC) platform, which coordinates to ^{99m}Tc and acts as the attachment point for the bioactive receptor-targeting vectors. The ethylenediamine coligand chelates to the remaining coordination sites on the Tc

metal centre. Whilst some of these HYNIC-based radiopharmaceuticals can be prepared from a single kit, ¹³ their structures remain ill-defined: ^{41,42} it is unknown whether HYNIC coordinates to Tc *via* the hydrazine group only, or as a bidentate ligand, *via* the hydrazine and pyridyl groups. Importantly, HYNIC-based bioconjugates are not known to provide isostructural Tc and Re derivatives, ^{41,42} and therefore cannot be used to develop dual ^{99m}Tc/¹⁸⁸Re theranostic tracers.

Compared with the existing 99m Tc-radiolabeled PSMA-targeted tracers, 99m Tc-MIP-1404, 99m Tc-PSMA-I&S, and 99m Tc-EDDA/HYNIC-iPSMA, the new $[^{99m}$ TcO₂($\mathbf{DP^{An}}$ -PSMAt)₂]⁺ and $[^{99m}$ TcO₂($\mathbf{DP^{MEP}}$ -PSMAt)₂]⁺ radiotracers demonstrate either increased or comparable blood clearance at 1–2 h after administration (Table 5). $[^{99m}$ TcO₂($\mathbf{DP^{An}}$ -PSMAt)₂]⁺ exhibits either decreased or comparable residualisation in murine liver compared to these other PSMA-targeted tracers.

These diphosphine chelators also enable simple, one-pot preparation of stable molecular radiotracers based on radioactive copper isotopes, such as 64 Cu for PET imaging, and its "theranostic" companion, 67 Cu ($t_{\frac{1}{2}}=61.9\,$ h; $100\%\,$ ß", $E_{\rm max}=561$ keV; $44\%\,$ γ , 185 keV), which emits ß" particles and has utility for systemic radiotherapy. 43 Critically, this allows application of the same diphosphine-peptide bioconjugate for theranostic radiopharmaceuticals that span both SPECT and PET imaging.

Concluding remarks

In summary, our new and highly versatile bis(phosphino) maleic anhydride platforms, DP^{An} and DP^{MEP} , enable facile preparation of diphosphine bioconjugates that can be simply radiolabelled with 99mTc for SPECT imaging, 64Cu for PET imaging and ¹⁸⁸Re for systemic radiotherapy, leading to the possibility of theranostic radiotracers. Importantly, these 99mTc radiotracers can be prepared in high radiochemical yields (≥95%) using a single step kit. This is a critical advance upon our prior DPPh and DPTol technology, as it allows for simple, one-step formulation of peptide-based 99mTc radiotracers, and presents new opportunities for economical molecular imaging using widely available ^{99m}Tc production infrastructure and γscintigraphy/SPECT cameras. We are currently expanding the application of $\mathbf{DP^{An}}$ and $\mathbf{DP^{MEP}}$ chemistry to other therapeutically relevant receptor targets, to develop a versatile suite of molecular SPECT, PET and radiotherapeutic tracers.

Edge Article Chemical Science

Author contributions

REN conceived research, designed experiments, undertook experimental work and drafted the manuscript; MTM and PGP conceived research, designed experiments and drafted the manuscript; INH, OWLC, AR, NP, ZY, JC and JDY undertook experimental work; TTP conceived research and undertook experimental work; IS, GIRC and LL contributed to experimental design; NV and HHT provided a 188W/188Re Oncobeta generator and provided expertise on its use and potential clinical applications.

Conflicts of interest

Some of the authors have submitted a patent application describing the intellectual property described herein. Nicholas Vetter is CEO of OncoBeta, who provide 188Re generators, including those used in this study. No other potential conflicts of interest relevant to this article exist.

Data availability

The data supporting this article, including abbreviations, experimental procedures, characterisation data, additional figures, chromatograms and spectra have been included as part of the SI. See DOI: https://doi.org/10.1039/d5sc02110c.

Acknowledgements

This research was supported by a Cancer Research UK Career Establishment Award (C63178/A24959), the EPSRC (EP/ S032789/1), the Cancer Research UK National Cancer Imaging Translational Accelerator Award (C4278/A27066), the EPSRC programme for Next Generation Molecular Imaging and Therapy with Radionuclides (EP/S019901/1), 'MITHRAS', the Wellcome Multiuser Equipment Radioanalytical Facility funded by Wellcome Trust (212885/Z/18/Z), and the Bristol Chemical Synthesis Centre for Doctoral Training, funded by EPSRC (EP/ L015366/1). SPECT/CT scanning equipment at KCL was funded by an equipment grant from the Medical Research Council (MR/X011992/1). The authors are grateful for research assistance with animal work from James Cormack, Harmony Blythin and Hagen Schmidt. We would like to thank Dr Paul J. Gates and the mass spectrometry facility of the University of Bristol, UK and Oscar Ayrton and the mass spectrometry facility of King's College London, UK for obtaining high-resolution mass spectra.

Notes and references

- $\dagger \; DP^{Ph}$ and DP^{Tol} and their derivatives have alternatively been abbreviated to "DP1" and "DP2", respectively in our prior report in a medical journal.20
- 1 M. Gabriel, C. Decristoforo, E. Donnemiller, H. Ulmer, C. W. Rychlinski, S. J. Mather and R. Moncayo, J. Nucl. Med., 2003, 44, 708-716.

- 2 M. S. Hofman, G. Kong, O. C. Neels, P. Eu, E. Hong and R. J. Hicks, J. Med. Imaging Radiat. Oncol., 2012, 56, 40-47.
- 3 A. Shinto, Curr. Trends Clin. Med. Imaging., 2017, 1, 91-94.
- 4 J. A. Jackson, I. N. Hungnes, M. T. Ma and C. Rivas, Bioconjugate Chem., 2020, 31, 483-491.
- 5 C. Rivas, J. A. Jackson, I. N. Hungnes and M. T. Ma, Compr. Coord. Chem. III, 2021, 9, 706-740.
- 6 M. Riondato, D. Rigamonti, P. Martini, C. Cittanti, A. Boschi, L. Urso and L. Uccelli, J. Med. Chem., 2023, 66, 4532-4547.
- 7 S. Liu and S. Chakraborty, Dalton Trans., 2011, 40, 6077-6086.
- 8 C. Schmidkonz, C. Hollweg, M. Beck, J. Reinfelder, T. I. Goetz, J. C. Sanders, D. Schmidt, O. Prante, T. Bäuerle, A. Cavallaro, M. Uder, B. Wullich, P. Goebell, T. Kuwert and P. Ritt, Prostate, 2018, 78, 54-63.
- 9 S. M. Hillier, K. P. Maresca, G. Lu, R. D. Merkin, J. C. Marquis, C. N. Zimmerman, W. C. Eckelman, J. L. Joyal and J. W. Babich, J. Nucl. Med., 2013, 54, 1369-1376.
- 10 S. Robu, M. Schottelius, M. Eiber, T. Maurer, J. Gschwend, M. Schwaiger and H. J. Wester, J. Nucl. Med., 2017, 58,
- 11 T. Maurer, S. Robu, M. Schottelius, K. Schwamborn, I. Rauscher, N. S. van den Berg, F. W. B. van Leeuwen, B. Haller, T. Horn, M. M. Heck, J. E. Gschwend, M. Schwaiger, H. J. Wester and M. Eiber, Eur. Urol., 2019, 75, 659-666.
- 12 I. O. Lawal, A. O. Ankrah, N. P. Mokgoro, M. Vorster, A. Maes and M. M. Sathekge, Prostate, 2017, 77, 1205-1212.
- 13 G. Ferro-Flores, M. Luna-Gutiérrez, B. Ocampo-García, C. Santos-Cuevas, E. Azorín-Vega, N. Jiménez-Mancilla, E. Orocio-Rodríguez, J. Davanzo and F. O. García-Pérez, Nucl. Med. Biol., 2017, 48, 36-44.
- 14 P. Bernal, J. L. Raoul, J. Stare, E. Sereegotov, F. X. Sundram, A. Kumar, J. M. Jeong, P. Pusuwan, C. Divgi, P. Zanzonico, G. Vidmar, J. Buscombe, T. T. M. Chau, M. M. Saw, S. Chen, R. Ogbac, M. Dondi and A. K. Padhy, Semin. Nucl. Med., 2008, 38, S40-S45.
- 15 A. Shinto, World J. Nucl. Med., 2017, 16, 1-2.
- 16 A. Shinto, M. Mallia, M. Kameswaran, K. Kamaleshwaran, Joseph, E. Radhakrishnan, I. R. Subramaniam, M. Sairam, S. Banerjee and A. Dash, World J. Nucl. Med., 2018, 17, 228-235.
- 17 J. Cardinale, F. L. Giesel, C. Wensky, H. G. Rathke, U. Haberkorn and C. Kratochwil, J. Nucl. Med., 2023, 64, 1069-1075.
- 18 I. N. Hungnes, F. Al-Salemee, P. J. Gawne, T. Eykyn, R. A. Atkinson, S. Y. A. Terry, F. Clarke, P. J. Blower, P. G. Pringle and M. T. Ma, Dalton Trans., 2021, 50, 16156-
- 19 I. N. Hungnes, T. T. Pham, C. Rivas, J. A. Jarvis, R. E. Nuttall, S. M. Cooper, J. D. Young, P. J. Blower, P. G. Pringle and M. T. Ma, Inorg. Chem., 2023, 62, 20608-20620.
- 20 T. T. Pham, I. N. Hungnes, C. Rivas, J. Cleaver, G. Firth, P. J. Blower, J. Sosabowski, G. J. R. Cook, L. Livieratos, J. D. Young, P. G. Pringle and M. T. Ma, J. Nucl. Med., 2024, 65, 1087-1094.

21 R. E. Nuttall, T. T. Pham, A. C. Chadwick, I. N. Hungnes, G. Firth, M. A. Heckenast, H. A. Sparkes, M. C. Galan, M. T. Ma and P. G. Pringle, *Inorg. Chem.*, 2023, **62**, 20582–20592.

Chemical Science

- 22 J. S. Lewis, J. Zweit, J. L. J. Dearling, B. C. Rooney and P. J. Blower, *Chem. Commun.*, 1996, 1093–1094.
- 23 J. S. Lewis, S. L. Heath, A. K. Powell, J. Zweit and P. J. Blower, J. Chem. Soc., Dalton Trans., 1997, 855–861.
- 24 C. M. Dundas, D. Demonte and S. Park, *Appl. Microbiol. Biotechnol.*, 2013, **97**, 9343–9353.
- 25 S. Bongarzone, T. Sementa, J. Dunn, J. Bordoloi, K. Sunassee, P. J. Blower and A. Gee, J. Med. Chem., 2020, 63, 8265–8275.
- 26 C. Müller and R. Schibli, J. Nucl. Med., 2011, 52, 1-4.
- 27 M. Fernández, F. Javaid and V. Chudasama, *Chem. Sci.*, 2018, 9, 790–810.
- 28 C. Imberti, S. Y. A. Terry, C. Cullinane, F. Clarke, G. H. Cornish, N. K. Ramakrishnan, P. Roselt, A. P. Cope, R. J. Hicks, P. J. Blower and M. T. Ma, *Bioconjugate Chem.*, 2017, 28, 481–495.
- 29 C. Kratochwil, P. Flechsig, T. Lindner, L. Abderrahim, A. Altmann, W. Mier, S. Adeberg, H. Rathke, M. Röhrich, H. Winter, P. K. Plinkert, F. Marme, M. Lang, H. U. Kauczor, D. Jäger, J. Debus, U. Haberkorn and F. L. Giesel, J. Nucl. Med., 2019, 60, 801–805.
- 30 D. R. Anton and R. H. Crabtree, *Organometallics*, 1983, 2, 621–627.
- 31 H. Gali, T. J. Hoffman, G. L. Sieckman, N. K. Owen, K. V. Katti and W. A. Volkert, *Bioconjugate Chem.*, 2001, 12, 354–363.

- 32 K. K. Kothari, H. Gali, K. R. Prabhu, N. Pillarsetty, N. K. Owen, K. V. Katti, T. J. Hoffman and W. A. Volkert, *Nucl. Med. Biol.*, 2002, **29**, 83–89.
- 33 F. Kampmeier, J. D. Williams, J. Maher, G. E. Mullen and P. J. Blower, *EJNMMI Res.*, 2014, 4, 1–10.
- 34 J. Roy, B. M. Warner, F. Basuli, X. Zhang, K. Wong, T. Pranzatelli, A. T. Ton, J. A. Chiorini, P. L. Choyke, F. I. Lin and E. M. Jagoda, *Cancer Biother. Radiopharm.*, 2020, 35, 284–291.
- 35 S. Piron, J. Verhoeven, E. De Coster, B. Descamps, K. Kersemans, L. Pieters, A. Vral, C. Vanhove and F. De Vos, Sci. Rep., 2021, 11, 1–10.
- 36 N. Heynickx, K. Herrmann, K. Vermeulen, S. Baatout and A. Aerts, *Nucl. Med. Biol.*, 2021, **98–99**, 30–39.
- 37 J.-K. Chung, J. Nucl. Med., 2002, 43, 1188-1200.
- 38 F. Man, L. Lim, A. Volpe, A. Gabizon, H. Shmeeda, B. Draper, A. C. Parente-Pereira, J. Maher, P. J. Blower, G. O. Fruhwirth and R. T. M. de Rosales, *Mol. Ther.*, 2019, 27, 219–229.
- 39 M. Benešová, U. Bauder-Wüst, M. Schäfer, K. D. Klika, W. Mier, U. Haberkorn, K. Kopka and M. Eder, *J. Med. Chem.*, 2016, **59**, 1761–1775.
- 40 M. Benesová, M. Schäfer, U. Bauder-Wüst, A. Afshar-Oromieh, C. Kratochwil, W. Mier, U. Haberkorn, K. Kopka and M. Eder, *J. Nucl. Med.*, 2015, **56**, 914–920.
- 41 R. C. King, M. B. U. Surfraz, S. C. G. Biagini, P. J. Blower and S. J. Mather, *Dalton Trans.*, 2007, 4998–5007.
- 42 L. K. Meszaros, A. Dose, S. C. G. Biagini and P. J. Blower, *Inorg. Chim. Acta*, 2010, 363, 1059–1069.
- 43 S. E. Rudd, J. Van Zuylekom, C. Cullinane, B. J. Blyth and P. S. Donnelly, *Chem. Sci.*, 2025, **16**, 3998–4005.